IEEE Access
Multidisciplinary ⋮ Rapid Review ⋮ Open Access Journal

Received 9 March 2023, accepted 22 March 2023, date of publication 27 March 2023, date of current version 30 March 2023.

Digital Object Identifier 10.1109/ACCESS.2023.3261960

RESEARCH ARTICLE

An Improved Quantitative Analysis Method of Oscillation Mode for DFIG-Based Wind Power Base With LCC-HVDC Transmission Considering Frequency Coupling Characteristic

HAIPAN LI, HENG NIAN, (Senior Member, IEEE), YIMING LIU, BIN HU, YUMING LIAO, AND MENG LI, (Graduate Student Member, IEEE)

College of Electrical Engineering, Zhejiang University, Hangzhou 310027, China

Corresponding author: Heng Nian (nianheng@zju.edu.cn)

This work was supported by the National Natural Science Foundation of China under Grant 51977194.

ABSTRACT The line-commutated converter-based high-voltage direct-current (LCC-HVDC) transmission has become one of the main forms to deliver wind power in China. However, due to the connections of a large number of power electronic devices (PEDs), there emerges a risk of sub/super-synchronous oscillations in the DFIG-based wind power base with LCC-HVDC transmission. The existing multi-node system analysis methods have ignored the frequency coupling characteristic (FCC) of PEDs, unable to obtain accurate oscillation characteristics. Besides, the relationship between the oscillation and multi-level factors has not been revealed yet. Therefore, this paper proposes an improved quantitative analysis method of oscillation mode which considers the FCC on the basis of the system admittance network model. Firstly, the impedance model of the system considering the FCC is established. Then, the improved quantitative analysis method of the oscillation mode considering the FCC is proposed and its steps are as follows. 1) To establish the system transfer function matrix considering the FCC, and determine the system stability accurately by the dominant oscillation mode; 2) To define the node oscillation participation factor, considering the effect of the coupling frequency, and quantify the participation degree of each node and identify the origin and weak point of oscillation; 3) To carry out multi-level oscillation mode sensitivity analysis. Finally, the oscillation characteristics and laws of the DFIG-based wind power base with LCC-HVDC transmission are studied, and the time-domain simulations in MATLAB/Simulink validate the analytical results.

INDEX TERMS LCC-HVDC, DFIG-based wind power, frequency coupling characteristic (FCC), quantitative analysis, oscillation mode.

I. INTRODUCTION

To achieve carbon emission peak and carbon neutrality, renewable energy sources such as wind and solar power have been developing rapidly in China in recent years and the installed capacity has been increasing year by year [1], [2]. However, China's renewable energy bases are mostly located in the northern area [3], which are far away from the eastern load centers. Therefore, it's urgent to adopt an efficient power transmission method for long-distance transmission of renewable energy power [4].

The line-commutated converter-based high-voltage direct-current (LCC-HVDC) transmission has become one of the main forms to deliver wind power due to its mature technology, large transmission capacity, and suitability for long-distance transmission [5], [6]. However, there are a large number of power electronic devices (PEDs) and a variety of control loops in the DFIG-based wind power

The associate editor coordinating the review of this manuscript and approving it for publication was Xiaodong Liang.

This work is licensed under a Creative Commons Attribution-NonCommercial-NoDerivatives 4.0 License.
For more information, see https://creativecommons.org/licenses/by-nc-nd/4.0/

base and the LCC-HVDC, which make dynamic interactions complex, and then cause a risk of sub/super-synchronous oscillations [7]. Therefore, it is of great importance to analyze the oscillation characteristics of the DFIG-based wind power base with LCC-HVDC transmission. It's noted that the oscillation characteristics are determined by the interactions among the DFIG-based wind farms, LCC-HVDC, and weak AC grid. And due to the frequency coupling characteristics (FCC) of both DFIG-based wind farms and LCC-HVDC [8], [9], the interactions become more complex, making it difficult to identify the origin and weak point of oscillation. As a result, there is an urgent need for a method that can analyze the oscillation characteristics accurately.

References [10] and [11] established the state space model of DFIG-based wind farms with LCC-HVDC transmission and investigated the oscillation characteristics through eigenvalue analysis. However, [10], [11] equated multiple wind farms to a single wind farm and only focused on the interaction between the wind farm and LCC-HVDC. When considering different wind farms, the number of system state variables increases rapidly, which makes the state space model more complex and would then lead to a "dimensional disaster" problem for the eigenvalue solution. In this way, there exists a limitation to the eigenvalue analysis method for applying multiple wind farms with LCC-HVDC transmission. References [12] and [13] established the impedance model of LCC-HVDC and analyzed the oscillation stability of DFIG-based wind farms with LCC-HVDC transmission by the impedance analysis method. However, the impedance analysis method only focuses on the stability of the interconnection port between wind farms and LCC-HVDC, and cannot obtain detailed information such as the origin, distribution, and weak point of oscillation.

Therefore, a method based on the s-domain node admittance matrix (SNAM) has been proposed to study the oscillation characteristics of a multi-node system. References [14] and [15] revealed that the oscillation stability of the system can be determined by the zeros of the SNAM determinant. In [16], the participation factor was used to determine the contribution of each node to the unstable harmonics in the grid-connected system to locate critical nodes. Reference [17] analyzed the effect of series compensation elements on the stability of DFIG-based wind farm grid-connected system by component sensitivity. However, the existing SNAM-based methods ignore the FCC of PEDs and cannot get the accurate oscillation characteristics of the system [8], [9]. Moreover, they only pay attention to the influence of components on stability but do not investigate the relationship between the oscillation and multi-level factors such as nodes, devices, and parameters in complex renewable energy power systems.

Hence, to analyze the oscillation characteristics accurately and to reveal the relationship between the oscillation and multi-level factors, this paper proposes an improved quantitative analysis method of oscillation mode which considers the FCC, based on the system admittance network model. The main contributions are as follows:

(1) The SNAM of the system considering FCC is constructed to contain the complete topology information and all oscillation modes, and so as to determine the oscillation stability accurately.

(2) Considering the effect of coupling frequency, the node oscillation participation factor corresponding to the oscillation mode is defined to quantify the participation information of each node and locate the main impact area of the oscillation mode.

(3) The relationship between the oscillation and multi-level factors is revealed through the multi-level oscillation mode sensitivity, which portrays the oscillation law of the system under multi-level factors.

The rest of this paper is organized as follows. System description and impedance modeling of the DFIG-based wind power base with LCC-HVDC transmission are given in Section II as a foundation of the following analysis. Then, the improved quantitative analysis method of oscillation mode which considers the FCC is proposed in Section III. Section IV investigates the oscillation characteristics and laws of the system and conducts time-domain simulations for verification. Finally, Section V concludes this paper.

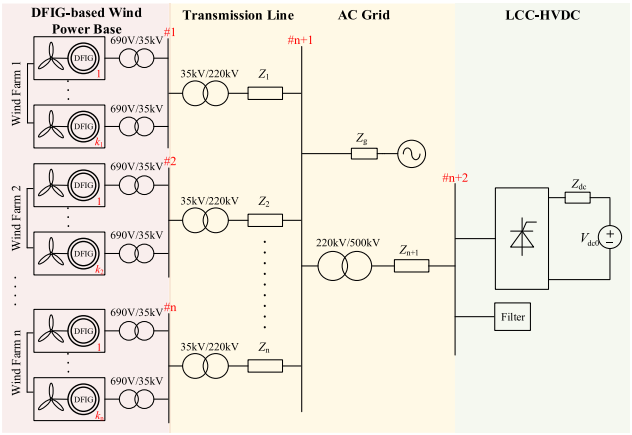

FIGURE 1. Schematic diagram of the DFIG-based wind power base with LCC-HVDC transmission.

II. IMPEDANCE MODELLING OF THE DFIG-BASED WIND POWER BASE WITH LCC-HVDC TRANSMISSION

This section introduces the structure of the system and then models the impedance of each part of the system in consideration of the FCC to lay a foundation for the subsequent analysis.

A. SYSTEM DESCRIPTION

Figure 1 shows the structure of the DFIG-based wind power base with LCC-HVDC transmission, which includes four parts, i.e., DFIG-based wind power base, transmission line, AC grid, and LCC-HVDC.

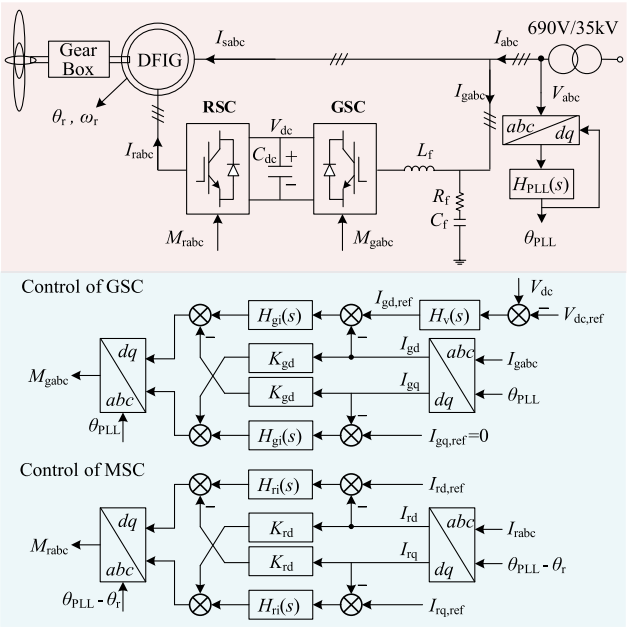

FIGURE 2. Circuit and control structure diagram of DFIG-based wind turbine.

The DFIG-based wind power base consists of n DFIG-based wind farms, each containing k_1, k_2, ..., k_n DFIG-based wind turbines connected in parallel. Each DFIG-based wind turbine gathers its power to the wind farm port via a 690V/35kV step-up transformer. All wind farms gather their power to the wind power base port via a 35kV/220kV step-up transformer and a 220kV transmission line. Then the wind power and the power from the AC grid are sent to the LCC-HVDC system port via a 220kV/500kV step-up transformer and a 500kV transmission line. Finally, the power is sent through LCC-HVDC with a DC voltage level of 400kV.

Where Z_1, Z_2, ..., Z_n are the 220kV transmission line impedances; Z_{n+1} is the 500kV transmission line impedance; Z_g is the AC grid equivalent impedance; Z_{dc} is the DC transmission line impedance; the filter is used to absorb the steady state harmonics on the AC side of the LCC-HVDC.

B. IMPEDANCE MODELING OF DFIG-BASED WIND POWER BASE

The basic unit of the DFIG-based wind power base is the DFIG-based wind turbine, whose main circuit and control block diagram is shown in Figure 2.

where $H_{PLL}(s)$ is the phase-locked loop PI regulator; $H_v(s)$ is the DC voltage loop PI regulator; $H_{gi}(s)$ is the GSC-side current loop PI regulator, K_{gd} is its decoupling factor; $H_{ri}(s)$ is the RSC-side current loop PI regulator, K_{rd} is its decoupling factor. L_f is the filter inductance, R_f is the filter resistance, C_f is the filter capacitor, C_{dc} is the DC bus capacitance, θ_r and ω_r are the rotor angle and rotor angular velocity, θ_{PLL} is the phase-locked angle, the symbols V, I and M denote the voltage component, the current component and the modulating signal output from the controller respectively, the subscript abc denotes the three-phase quantity, the subscripts g, s, r, and dc denote the grid-side, stator-side, rotor-side, and dc-side components respectively.

The impedance model of a DFIG-based wind turbine considering FCC can be expressed as a 2 × 2 admittance matrix [18].

$$\begin{bmatrix} I_p(s) \\ I_n(s') \end{bmatrix} = \underbrace{\begin{bmatrix} Y_{11}(s) & Y_{12}(s') \\ Y_{21}(s) & Y_{22}(s') \end{bmatrix}}_{Y_{DFIG}} \begin{bmatrix} V_p(s) \\ V_n(s') \end{bmatrix} \tag{1}$$

where s is the complex frequency domain variable, $s' = s - j4\pi f_1$, $f_1 = 50$Hz; $Y_{11}(s)$ and $Y_{22}(s')$ are the positive and negative sequence admittances, respectively; $Y_{21}(s)$ and $Y_{12}(s')$ are the frequency coupling terms of the positive and negative sequence admittances, respectively.

The existing DFIG-based wind turbine impedance models are all based on the single-unit-ideal grid, where the initial phase of the port voltage is assumed to be 0° during the modeling process. However, in real wind farms, the initial phase of the voltage at the ports of each DFIG-based wind turbine can hardly meet the assumption due to the influence of transmission lines, etc. Since ignoring the initial phase may misjudge the system stability (see Appendix A for details), this paper further considers the effect of the initial phase φ_{v0} of the port voltage to modify the impedance model. The results are shown in (2) and it can be found that the initial phase φ_{v0} only affects the phase of the non-diagonal terms.

$$\mathbf{Y}_{DFIG} = \begin{bmatrix} Y_{11}(s) & e^{j2\varphi_{v0}} Y_{12}(s') \\ e^{-j2\varphi_{v0}} Y_{21}(s) & Y_{22}(s') \end{bmatrix} \tag{2}$$

This paper focuses on the interactions between wind farms in the DFIG-based wind power base. To simplify the analysis, it is assumed that the structure, parameters, and operating states of all wind turbines in the same wind farm shown in Figure 1 are identical. Therefore, the impedance model of the wind farm can be expressed as (3), where k is the number of wind turbines in the wind farm.

$$\mathbf{Y}_{WF} = k\mathbf{Y}_{DFIG} \tag{3}$$

C. IMPEDANCE MODELING OF LCC-HVDC

The circuit and control block diagram of LCC-HVDC are shown in Figure 3. Due to DC voltage control, the influence of inverter on the impedance model of LCC-HVDC can be approximated as a constant voltage source V_{dc0} [7], [9], [19]. where $H_{PLL\_L}(s)$ is the phase-locked loop PI regulator; $H_{im}(s)$ is the DC current measurement link including constant gain and first order low pass filter; $H_i(s)$ is the DC current loop PI regulator. L_d is the DC link inductance, R_d is the DC link resistance and C_d is the DC line capacitor [10]. The AC side filter Z_f mainly consists of 11th and 13th-order tuned filters and a 24th-order high-pass damping filter.

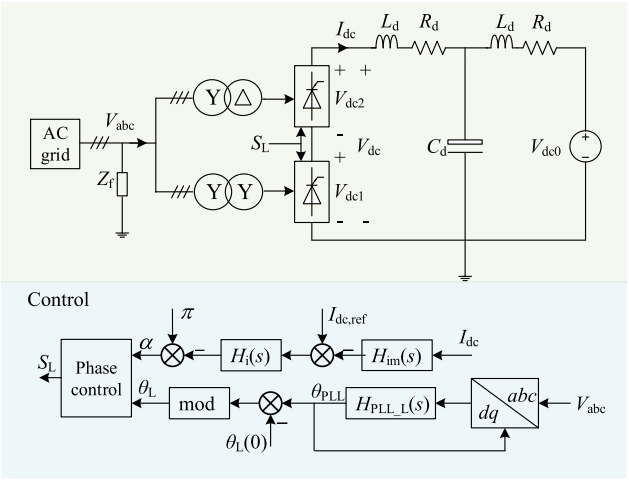

FIGURE 3. Circuit and control structure diagram of LCC-HVDC.

In [9], an impedance model for the LCC-HVDC rectifier station is established. Similarly, it can be expressed as a 2 × 2 admittance matrix as shown in (4) after considering the initial phase φ_{v1} of the AC port voltage.

$$\mathbf{Y}_{\mathrm{LCC}} = \begin{bmatrix} Y_{11}(s) & e^{j2\varphi_{v1}} Y_{12}(s') \\ e^{-j2\varphi_{v1}} Y_{21}(s) & Y_{22}(s') \end{bmatrix} \tag{4}$$

D. IMPEDANCE MODELING OF TRANSMISSION LINE AND AC GRID

The transmission line can be modeled using either a T-model equivalent circuit or a π-model equivalent circuit [20]. Considering that the effect of the shunt capacitance of the transmission line on the dynamic characteristics of the system is small and can be neglected [21], the admittance model of the transmission line is simplified as (5)

$$\mathbf{Y}_{\mathrm{L}} = \begin{bmatrix} 1/(R_{\mathrm{L}} + sL_{\mathrm{L}}) & 0 \\ 0 & 1/(R_{\mathrm{L}} + s'L_{\mathrm{L}}) \end{bmatrix} \tag{5}$$

where R_{L} is the line resistance and L_{L} is the line inductance.

Similarly, the AC grid can be expressed in terms of the equivalent inductance L_{g}.

$$\mathbf{Y}_{\mathrm{g}} = \begin{bmatrix} 1/sL_{\mathrm{g}} & 0 \\ 0 & 1/s'L_{\mathrm{g}} \end{bmatrix} \tag{6}$$

III. QUANTITATIVE ANALYSIS METHOD OF OSCILLATION MODE CONSIDERING FCC

As can be seen from Figure 1, the oscillation characteristics of the system are related to the interactions among all wind farms, the AC grid, and the LCC-HVDC, and are also influenced by the transmission line. References [8] and [9] point out that the FCC of both the DFIG-based wind farm and the LCC-HVDC would lead to a more complex analysis of the oscillation characteristics. Existing oscillation analysis methods cannot analyze the oscillation characteristics and laws of the system accurately, making it difficult to identify the origin and weak point of oscillation. Therefore, this section proposes an improved quantitative analysis method of oscillation mode which considers the FCC, based on the system admittance network model.

Firstly, the system transfer function matrix considering the FCC is established to obtain the oscillation mode to determine the system stability; then, considering the effect of coupling frequency, the node oscillation participation factor is established to assess the participation degree of each node accurately and to locate the main influence area of the oscillation mode; finally, the sensitivity analysis of the oscillation modes is carried out by establishing multi-level oscillation mode sensitivity to quantify the relationships between the oscillation modes and multi-level factors such as nodes, devices, and parameters.

A. OSCILLATION MODE OF THE SYSTEM

As shown in Figure 1, the system contains $n + 2$ nodes. According to the system topology, the system's current-voltage relationship considering the FCC can be represented by the SNAM [22], as shown in (7), as shown at the bottom of the next page. Where the SNAM is noted as $\mathbf{Y}_{\mathrm{SN}}(s)$ which is a 2(n+2)×2(n+2) matrix; the terms in the node injection current vector matrix $\mathbf{I}(s)$ and the node voltage vector matrix $\mathbf{U}(s)$ are $\mathbf{I}_i = [I_{\mathrm{p}i}, I_{\mathrm{n}i}]^{\mathrm{T}}$, $\mathbf{U}_i = [U_{\mathrm{p}i}, U_{\mathrm{n}i}]^{\mathrm{T}}$, $i = 1, \ldots, n+2$.

Taking $\mathbf{I}(s)$ as the input and $\mathbf{U}(s)$ as the output, the inverse matrix of SNAM is the equivalent transfer function matrix of the system, as shown in (8). Therefore, the oscillation modes of the system can be obtained by solving the zeros of the SNAM determinant [14], [15].

$$\mathbf{U}(s) = \mathbf{Y}_{\mathrm{SN}}(s)^{-1}\mathbf{I}(s) = \frac{\mathbf{Y}_{\mathrm{SN}}(s)^*}{\det[Y_{\mathrm{SN}}(s)]}\mathbf{I}(s) \tag{8}$$

Due to the consideration of FCC, the oscillation modes will appear in pairs.

$$\det[\mathbf{Y}_{\mathrm{SN}}(s_{\mathrm{k}})] = 0 \tag{9}$$

where s_{k} is the kth pair of oscillation modes, which can be expressed as $s_{\mathrm{k},1} = -\sigma_{\mathrm{k}} + j2\pi f_{\mathrm{k},1}$ and $s_{\mathrm{k},2} = -\sigma_{\mathrm{k}} + j2\pi f_{\mathrm{k},2}$; σ_{k} is the damping of the pair of oscillation modes; $f_{\mathrm{k},1}$ and $f_{\mathrm{k},2}$ are the oscillation frequencies of the pair of oscillation modes, both of which satisfy $f_{\mathrm{k},1} = 2f_1 - f_{\mathrm{k},2}$. Since each pair of oscillation modes satisfies the above relationship, $s_{\mathrm{k},1}$ can be selected to analyze the oscillation characteristics and laws of the pair. The system is stable when the oscillation modes of the system are all located in the left half-plane of the complex plane.

B. NODE OSCILLATION PARTICIPATION FACTOR

Based on the obtained oscillation modes, the node oscillation participation factor is further established. Taking the oscillation mode s_{k} as an example, the oscillation mode s_{k} is substituted into SNAM to obtain the complex constant

matrix $\mathbf{Y}_{SN}(s_k)$. On the basis of the eigenvalue decomposition theory [23], $\mathbf{Y}_{SN}(s_k)$ is diagonalized and then obtain (10).

$$\mathbf{Y}_{SN}(s_k) = \mathbf{R} \times \Lambda \times \mathbf{L}^T \tag{10}$$

where $\Lambda = \text{diag}(\lambda_1, \lambda_2, \ldots, \lambda_{2(n+2)})$ is the matrix of eigenvalues under the oscillation mode s_k; $\mathbf{R}=[\mathbf{R}_1, \mathbf{R}_2, \ldots, \mathbf{R}_{2(n+2)}]$ is the corresponding matrix of right eigenvectors and $\mathbf{L}=[L_1^T, L_2^T, \ldots, L_{2(n+2)}^T]$ is the corresponding matrix of left eigenvectors; matrices $\mathbf{R}$ and $\mathbf{L}$ satisfy $\mathbf{R}^{-1} = \mathbf{L}^T$.

Since the determinant of $\mathbf{Y}_{SN}(s_k)$ is zero, there must exist a zero eigenvalue (denoted as λ_{sk}) for $\mathbf{Y}_{SN}(s_k)$. Substituting (10) into (8) yields (11).

$$\mathbf{L}^T\mathbf{U}(s_k) = \Lambda^{-1}\mathbf{L}^T\mathbf{I}(s_k) \tag{11}$$

Define the mode voltage $\mathbf{V}(s) = \mathbf{L}^T\mathbf{U}(s)$ and the mode current $\mathbf{J}(s) = \mathbf{L}^T\mathbf{I}(s)$ according to (11), then the relationship between the mode voltage and the mode current corresponding to λ_{sk} satisfies (12).

$$V_{sk} = \lambda_{sk}^{-1} J_{sk} \tag{12}$$

Since $\lambda_{sk} = 0$, the mode current J_{sk} will excite a relatively large mode voltage V_{sk} at this point, and the voltage at each node of the system will be dominated by this mode voltage. Therefore, the relationship between node voltage and node injection current can be written as (13).

$$\begin{aligned}\mathbf{U}(s_k) = RV(s_k) &\approx \mathbf{R}_{sk} V_{sk} = \mathbf{R}_{sk}\lambda_{sk}^{-1} J_{sk} \\ &= \lambda_{sk}^{-1}\mathbf{R}_{sk}\mathbf{L}_{sk}\mathbf{I}(s_k) = \lambda_{sk}^{-1} P_{sk}\mathbf{I}(s_k)\end{aligned} \tag{13}$$

where $\mathbf{R}_{sk}$ and $\mathbf{L}_{sk}$ are the right and left eigenvectors corresponding to λ_{sk}; the diagonal elements of $\mathbf{P}_{sk}$ not only measure the participation degree of each node in the oscillation mode s_k but also reflect the influence degree of each node by the oscillation mode s_k. Taking the normalized diagonal elements as the node oscillation participation factors, the oscillation participation factor of node i is defined as (14) due to the consideration of FCC.

$$P_{pui} = \frac{|P_{sk(2i-1)(2i-1)}| + |P_{sk(2i)(2i)}|}{\sum_{j=1}^{2(n+2)} |P_{skjj}|} \tag{14}$$

where P_{skjj} is the jth row and jth column element of $\mathbf{P}_{sk}$.

C. OSCILLATION MODE SENSITIVITY

The general form of sensitivity is defined as follows:

$$S(x) = \frac{\partial y}{\partial x} \tag{15}$$

It can be seen that the sensitivity can portray the relationship between two variables and quantify the influence degree and law in x on y. Therefore, in order to analyze the relationships between the oscillation modes and the multi-level factors (i.e., nodes, devices, and parameters), this section establishes the multi-level oscillation mode sensitivity to develop the oscillation mode sensitivity analysis.

1) NODE-LEVEL OSCILLATION MODE SENSITIVITY

The node-level oscillation mode sensitivity describes the relationship between the node admittance matrix and the oscillation mode of the system and quantifies the influence degree and law in the elements of the node admittance matrix on the oscillation mode. According to (15), taking the oscillation mode s_k as an example, the node-level oscillation mode sensitivity is defined as follows:

$$\mathbf{S}(\mathbf{Y}_{SN}) = \frac{\partial s_k}{\partial \mathbf{Y}_{SN}} \tag{16}$$

where the element in row i and column j of $\mathbf{S}(\mathbf{Y}_{SN})$ represents the sensitivity of the oscillation mode s_k to Y_{ij} in $\mathbf{Y}_{SN}$.

Since there is no explicit expression for the oscillation mode s_k, it is impossible to derive the expression for the node-level oscillation mode sensitivity. Its implicit expression is derived below.

From (9), the oscillation mode s_k is the zero of the SNAM determinant, so the following equation must exist.

$$\begin{cases} Z_{SNii}(s_k, \mathbf{Y}_{SN}) = \mathbf{I}_i^T \mathbf{Z}_{SN}(s_k)\mathbf{I}_i = \mathbf{I}_i^T \mathbf{Y}_{SN}(s_k)^{-1}\mathbf{I}_i = \infty \\ Y_{SNii}(s_k, \mathbf{Y}_{SN}) = 1/Z_{SNii}(s_k, \mathbf{Y}_{SN}) = 0 \end{cases} \tag{17}$$

where $Z_{SNii}(s_k, \mathbf{Y}_{SN})$ and $Y_{SNii}(s_k, \mathbf{Y}_{SN})$ are the port impedance and admittance, respectively, and $\mathbf{I}_i$ is a one-dimensional column vector, where the ith element is 1 and the remaining elements are 0.

Applying the implicit function derivative rule [24] to the port admittance, the node-level oscillation mode sensitivity

$$\begin{bmatrix} \mathbf{I}_1 \\ \vdots \\ \mathbf{I}_n \\ \mathbf{I}_{n+1} \\ \mathbf{I}_{n+2} \end{bmatrix} = \underbrace{\begin{bmatrix} \mathbf{Y}_{WF1} + \mathbf{Y}_{L1} & \cdots & 0 & -\mathbf{Y}_{L1} & 0 \\ \vdots & \vdots & \vdots & \vdots & \vdots \\ 0 & \cdots & \mathbf{Y}_{WFn} + \mathbf{Y}_{Ln} & -\mathbf{Y}_{Ln} & 0 \\ -\mathbf{Y}_{L1} & \cdots & -\mathbf{Y}_{Ln} & \sum_{i=1}^{n+1} Y_{Li} + \mathbf{Y}_g & -\mathbf{Y}_{L(n+1)} \\ 0 & \cdots & 0 & -\mathbf{Y}_{L(n+1)} & \mathbf{Y}_{LCC} + \mathbf{Y}_{L(n+1)} \end{bmatrix}}_{\mathbf{Y}_{SN}} \begin{bmatrix} \mathbf{U}_1 \\ \vdots \\ \mathbf{U}_n \\ \mathbf{U}_{n+1} \\ \mathbf{U}_{n+2} \end{bmatrix} \tag{7}$$

is collated as follows.

$$\frac{\partial s_k}{\partial \mathbf{Y}_{SN}} = -\frac{\mathbf{Z}_{SN}^T \mathbf{I}_i \mathbf{I}_i^T \mathbf{Z}_{SN}^T}{\mathbf{I}_i^T \mathbf{Z}_{SN} \frac{\partial \mathbf{Y}_{SN}(s_k, \mathbf{Y}_{SN})}{\partial s_k} \mathbf{Z}_{SN} \mathbf{I}_i} \tag{18}$$

Note that: due to the consideration of FCC, the node-level oscillation mode sensitivity $\mathbf{S}(\mathbf{Y}_{SN})$ is a $2(n+2)\times 2(n+2)$ matrix whose diagonal elements reflect the influence degree and law of each node on the oscillation mode s_k.

2) DEVICE-LEVEL OSCILLATION MODE SENSITIVITY

The device-level oscillation mode sensitivity quantifies the influence degree and law of each device in the system on the oscillation mode. Depending on how they are connected in the system, the devices can be divided into parallel and series devices. Taking the system shown in Figure 1 as an example, the parallel devices include the DFIG-based wind farm, LCC-HVDC, and AC grid; the series devices include the 220 kV transmission line and the 500 kV transmission line.

From (7), it can be seen that the parallel and series devices have different effects on the node admittance matrix, so based on the node-level oscillation mode sensitivity $\mathbf{S}(\mathbf{Y}_{SN})$, the parallel device-level oscillation mode sensitivity and the series device-level oscillation mode sensitivity are established respectively.

Since parallel devices only affect the main diagonal elements of the connected nodes, the sensitivity of the parallel device connected to node i to the oscillation mode s_k is defined as follows.

$$\mathbf{S}(\mathbf{Y}_P) = \mathbf{S}(\mathbf{Y}_{SN})_{ii} \circ \frac{\partial \mathbf{Y}_{SNii}}{\partial \mathbf{Y}_P} \tag{19}$$

where $\circ$ represents Hadamard product, $\mathbf{Y}_P$ is the parallel device admittance matrix and $\mathbf{S}(\mathbf{Y}_P)$ is a 2×2 matrix.

While series devices affect not only the main diagonal elements of the connected nodes but also the corresponding non-diagonal elements of the connected nodes, thus the sensitivity of the series devices between node i and node j to the oscillation mode s_k is defined as follows.

$$\begin{aligned}\mathbf{S}(\mathbf{Y}_S) = {} & \mathbf{S}(\mathbf{Y}_{SN})_{ii} \circ \frac{\partial \mathbf{Y}_{SNii}}{\partial \mathbf{Y}_S} + \mathbf{S}(\mathbf{Y}_{SN})_{jj} \circ \frac{\partial \mathbf{Y}_{SNjj}}{\partial \mathbf{Y}_S} \\ & + \mathbf{S}(\mathbf{Y}_{SN})_{ij} \circ \frac{\partial \mathbf{Y}_{SNij}}{\partial \mathbf{Y}_S} + \mathbf{S}(\mathbf{Y}_{SN})_{ji} \circ \frac{\partial \mathbf{Y}_{SNji}}{\partial \mathbf{Y}_S}\end{aligned} \tag{20}$$

where $\mathbf{Y}_S$ is the series device admittance matrix and $\mathbf{S}(\mathbf{Y}_S)$ is a 2×2 matrix.

3) PARAMETER-LEVEL OSCILLATION MODE SENSITIVITY

The parameter-level oscillation mode sensitivity quantifies the influence degree and law of each parameter of the device on the oscillation mode. Combined with (19) and (20), the sensitivity of the parameter p of the device $\mathbf{Y}_P$ to the oscillation mode s_k can be defined as follows.

$$S(p) = \sum\sum \mathbf{S}(\mathbf{Y}_P) \circ \frac{\partial \mathbf{Y}_P}{\partial p} \tag{21}$$

The multi-level oscillation mode sensitivity quantifies the influence degree and law of multi-level factors (i.e., nodes, devices, and parameters) on the damping and oscillation frequency of the oscillation mode s_k. After normalization, the larger the absolute value of the real part of the oscillation mode sensitivity, the greater the influence of the corresponding node, device, and parameter on the damping of the oscillation mode, and if the value is negative, then increasing the factor can make the oscillation mode s_k shift left in the complex plane and improve the stability margin of the oscillation mode s_k; while the imaginary part reflects the influence of the factor on the oscillation frequency of the oscillation mode. Therefore, the multi-level oscillation mode sensitivity can be used to reveal the sensitive factors affecting the oscillation mode s_k hierarchically.

IV. STUDY OF THE OSCILLATION CHARACTERISTICS AND LAWS OF THE SYSTEM

In this section, the proposed improved method is used to investigate the oscillation characteristics and laws of the system shown in Figure 1. To facilitate analysis, let $n = 4$, i.e. the DFIG-based wind power base contains four wind farms.

A. ANALYSIS OF THE INTERACTION BETWEEN THE SAME WIND FARMS AND LCC-HVDC

Parameters for the four wind farms and their connecting lines are assumed to be identical, of which each wind farm is equipped with 50 turbines and the turbine parameters are shown in Table 7; assuming that the AC grid is weak, then the equivalent impedance of the grid Z_g is 93.08Ω, corresponding to an SCR of 2; the LCC-HVDC parameters are shown in Table 8; the four wind farms are 70km away from the 220kV bus and the length of 500kV transmission line is 200km. The transmission line parameters are shown in Table 9.

1) OSCILLATION MODE OF THE SYSTEM

First, the SNAM of the system is established according to (7); then, all the oscillation modes of the system in the frequency range of 0∼100Hz are solved and the results are listed in Table 1. It can be seen that there are five pairs of oscillation modes in the system, among which the real part of the oscillation mode 1 is greater than 0, which is an unstable oscillation mode, indicating that the system is unstable. And the results show that there are 31.18Hz and 68.82Hz oscillation components.

The simulation model is built in MATLAB/Simulink for verification. Figure 4 gives the waveforms of the LCC DC voltage and the node 6 AC voltage. The system operates stably from 2.5s to 3s, while turns to be unstable as the PLL proportional gain of LCC-HVDC changes from 60 to 48 at 3s. FFT analysis of the node 6 AC voltage during 4s to 5s is carried out and the results are shown in Figure 5. There are oscillation components of 31Hz and 69Hz, which are consistent with the oscillation mode 1 in Table 1.

TABLE 1. Oscillation mode of the system.

Oscillation mode	Sub-synchronous band	Super-synchronous band
1	2.56+j31.18×2π	2.56+j68.82×2π
2	-17.36+j47.45×2π	-17.36+j52.55×2π
3	-43.50+j49.76×2π	-43.50+j50.24×2π
4	-12.83+j46.32×2π	-12.83+j53.68×2π
5	-1.61+j0.77×2π	-1.61+j99.23×2π

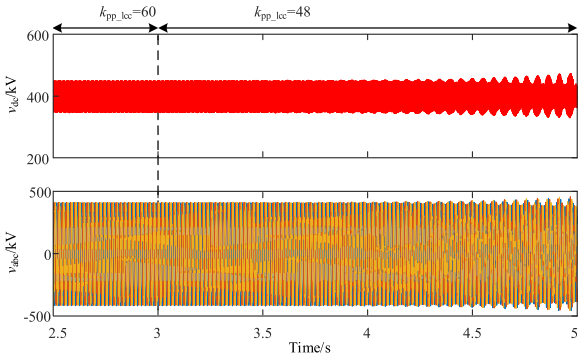

FIGURE 4. Time domain simulation waveform of system.

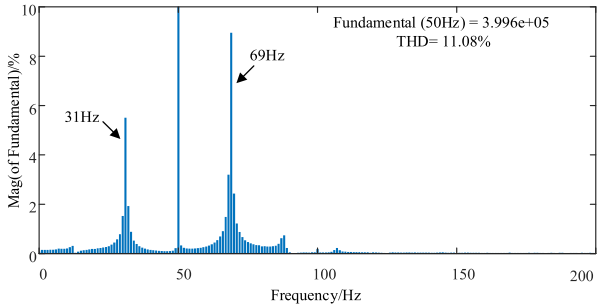

FIGURE 5. FFT analysis chart of Node 6 voltage during 4s to 5s.

TABLE 2. Node Oscillation Participation factors.

Node\s_k	s_1	s_2	s_3	s_4	s_5
1	0.1648	0.1594	0.1841	0.1713	0.1903
2	0.1648	0.1594	0.1841	0.1713	0.1903
3	0.1648	0.1594	0.1841	0.1713	0.1903
4	0.1648	0.1594	0.1841	0.1713	0.1903
5	0.1582	0.1599	0.1486	0.1535	0.1449
6	0.1825	0.2023	0.1152	0.1615	0.0938

2) NODE OSCILLATION PARTICIPATION FACTOR ANALYSIS

The node oscillation participation factors for the five pairs of oscillation modes are calculated according to (10), (13), and (14), and the normalized results are shown in Table 2.

As the four wind farms share the same parameters, their node oscillation participation factors in each pair of oscillation modes are identical, indicating the same degrees of participation. Node 6 shows the largest oscillation participation factor in oscillation modes 1 and 2, which means that the LCC-HVDC rectifier station connected to node 6 is most involved in oscillation modes 1 and 2; Nodes 1 to 4 in oscillation modes 3 to 5 show the largest the oscillation participation factors, indicating that the wind farms connected to nodes 1 to 4 are most involved in oscillation modes 3 to 5.

TABLE 3. Oscillation mode of the system.

Oscillation mode	Sub-synchronous band	Super-synchronous band
1	2.48+j31.19×2π	2.48+j68.81×2π
2	-17.35+j47.45×2π	-17.35+j52.55×2π
3	-43.57+j49.75×2π	-43.57+j50.25×2π
4	-12.82+j46.32×2π	-12.82+j53.68×2π
5	-2.87+j0.98×2π	-2.87+j99.02×2π

B. ANALYSIS OF THE INTERACTION BETWEEN THE DIFFERENT WIND FARMS AND LCC-HVDC

In practice, the configuration of each wind farm and the connection line parameters are different. It is assumed that: wind farms 1-4 are equipped with 75, 75, 25, and 25 wind turbines, respectively; wind farms 1-4 are 40km, 100km, 40km, and 100km away from the 220kV bus, respectively; other parameters remain unchanged.

1) OSCILLATION MODE OF THE SYSTEM

The calculation solutions for all oscillation modes in the 0-100Hz band of the sending system are listed in Table 3. Compared with Table 1, as configuration and connection line parameters of wind farms change, oscillation modes 1 to 4 suffer slight changes while oscillation mode 5 changes significantly. The presence of unstable oscillation modes indicates that the system is unstable, with oscillation components of 31.19Hz and 68.81Hz.

Similarly, the results of the oscillation mode analysis are verified by time-domain simulation, and the corresponding time-domain simulation waveform plots and FFT analysis results are shown in Figure 6 and Figure 7. It can be seen that the system is unstable, where oscillation components are 31Hz and 69Hz and are consistent with oscillation mode 1 in Table 3.

2) NODE OSCILLATION PARTICIPATION FACTOR ANALYSIS

The node oscillation participation factors for the five pairs of oscillation modes are calculated according to (10), (13), and (14), and the normalized results are shown in Table 4.

Compared with Table 2, changes in wind farm configuration and connection line parameters barely affect the degree of oscillation participation for nodes 5 and 6. In comparison among oscillation participation factors for nodes 1 to 4, it can be seen that for oscillation modes 1, 3, 4, and 5, the

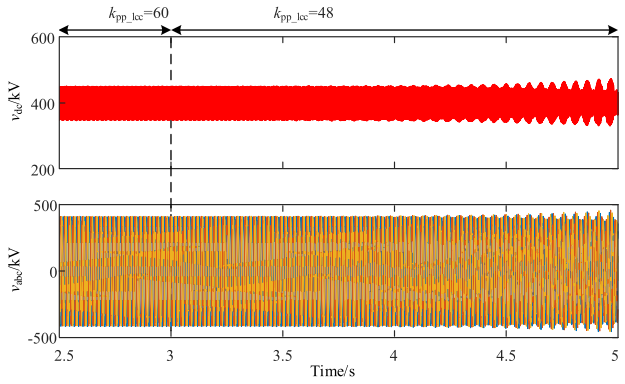

FIGURE 6. Time domain simulation waveform of system.

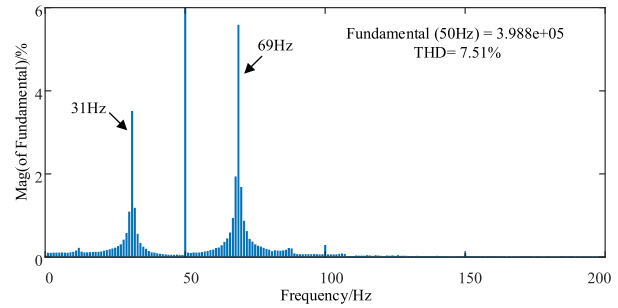

FIGURE 7. FFT analysis chart of Node 6 voltage during 4s to 5s.

TABLE 4. Node Oscillation Participation factors.

Node\s_k	s_1	s_2	s_3	s_4	s_5
1	0.1638	0.1596	0.1730	0.1682	0.1664
2	0.1729	0.1589	0.2451	0.1939	0.2811
3	0.1600	0.1598	0.1540	0.1581	0.1484
4	0.1628	0.1595	0.1684	0.1658	0.1607
5	0.1582	0.1599	0.1461	0.1531	0.1417
6	0.1824	0.2023	0.1133	0.1609	0.1017

participation degree of each wind farm is influenced by the length of the connection line and the number of turbines. While for oscillation mode 2, the participation degree of each wind farm is hardly influenced by the length of the connection line and the number of turbines.

The above analysis shows that there is a risk of sub/super-synchronous oscillations in the system. In the dominant oscillation mode 1, LCC-HVDC has the greatest participation and the participation of each wind farm is mainly related to the distance of the connection line and the number of turbines (i.e., the further the wind farm is from the 220kV bus and the more turbines there are, the greater the participation).

C. ANALYSIS OF MULTI-LEVEL OSCILLATION MODE SENSITIVITY

1) NODE-LEVEL OSCILLATION MODE SENSITIVITY

The sensitivity of each node of the system to the oscillation modes in Table 1 is calculated according to (18), whose magnitude reflects the influence degree of each node on oscillation mode s_k. Since the influence degree of each node on oscillation mode s_k is equivalent to the participation degree of each node in oscillation mode s_k, the normalized results of the magnitude of node-level oscillation mode sensitivity are the same as in Table 2.

It can be seen that at the node level, oscillation modes 1 and 2 are mainly influenced by node 6, and oscillation modes 3 to 5 are mainly influenced by nodes 1 to 4.

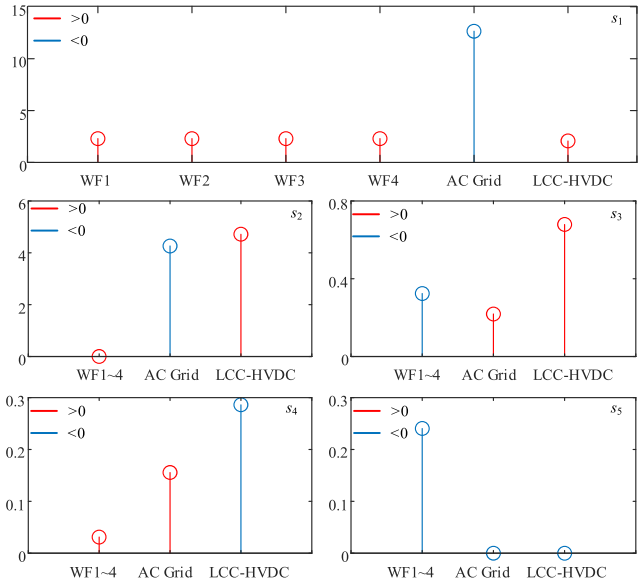

FIGURE 8. Parallel device sensitivity (Y-units: -1/s).

2) DEVICE-LEVEL OSCILLATION MODE SENSITIVITY

a: PARALLEL DEVICE OSCILLATION MODE SENSITIVITY

The sensitivities of each wind farm, AC grid, and LCC-HVDC are calculated according to (19). The standardized results are shown in Figure 8.

It can be seen that changes in the AC grid equivalent admittance have significant effects on oscillation modes 1 and 2, slight effects on oscillation modes 3 and 4, and no effects on oscillation mode 5. For the dominant oscillation mode 1, the sensitivity of the AC grid equivalent admittance is less than 0, indicating that system damping and stability increase as the AC grid equivalent admittance increases. Since the configurations of the four wind farms are identical, their sensitivities are equal. For dominant oscillation mode 1, the sensitivities of wind farms and LCC-HVDC are greater than 0, indicating that the damping decreases and the stability diminishes as their admittances increase.

b: SERIES DEVICE OSCILLATION MODE SENSITIVITY

The sensitivities of the transmission lines are calculated according to (20). The standardized results are shown in Figure 9. It can be seen that for the dominant oscillation mode 1, the sensitivity of the 500kV transmission line

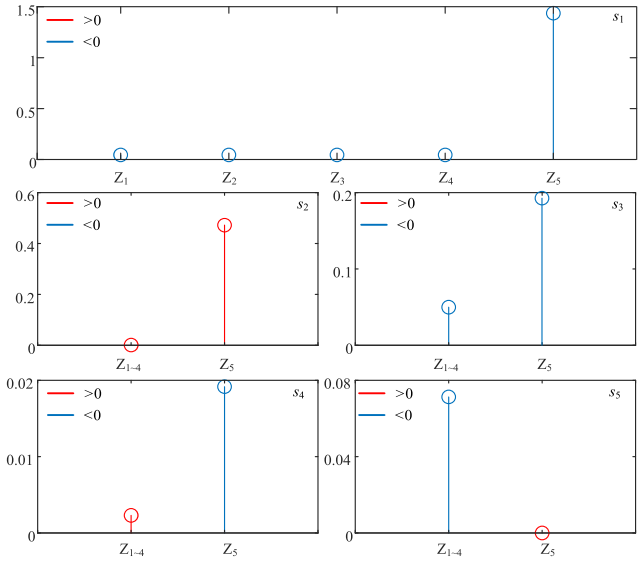

FIGURE 9. Series device sensitivity (Y-units: -1/s).

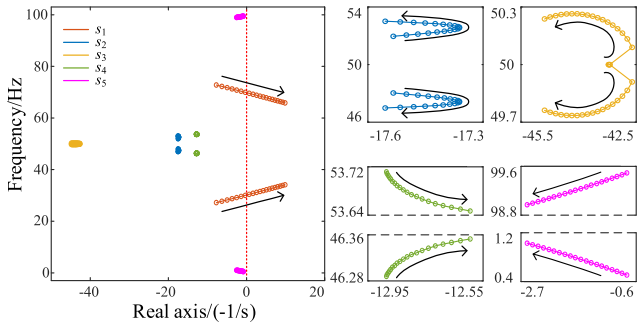

FIGURE 10. System oscillation mode trajectories diagram (Wind farm).

Z_5 is less than 0, indicating that as the length of the 500kV transmission line increases, the damping and stability increase.

c: VERIFICATION OF THE DEVICE-LEVEL SENSITIVITY

The wind farm, AC grid, and 500kV transmission line are selected to verify the accuracy and validity of the above sensitivity analysis results.

Since the wind farm admittance is proportional to the number of wind turbines, the results of the wind farm sensitivity analysis can be verified by changing the number of wind turbines. When the number of wind turbines in a wind farm increases from 5 to 100, the trajectories of the oscillation modes change as shown in Figure 10.

As Figure 10 shows, as the number of turbines increases, oscillation modes 1, 3, and 5 are significantly affected, while oscillation modes 2 and 4 are slightly affected; oscillation mode 1 gradually shifts to the right, the damping and stability decrease, which are consistent with the results of the sensitivity analysis. When the number of turbines increases to 40, oscillation mode 1 enters the right half-plane and the system becomes unstable.

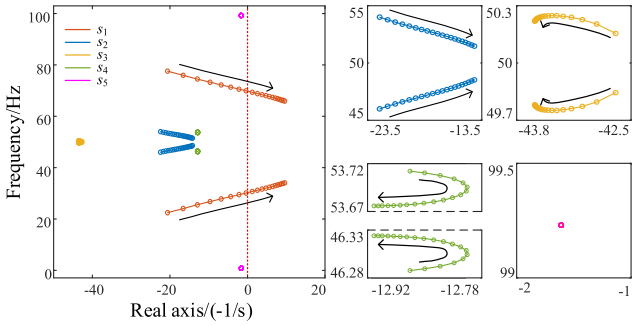

FIGURE 11. System oscillation mode trajectories diagram (AC Grid).

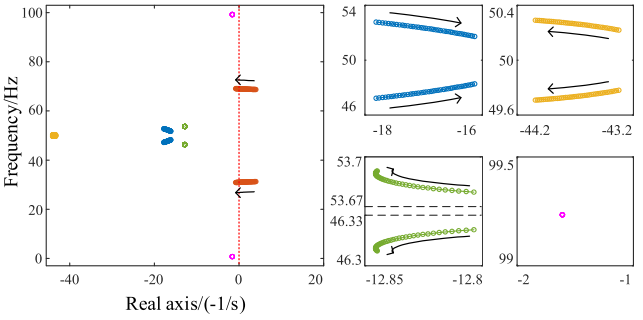

FIGURE 12. System oscillation mode trajectories diagram (500kV line).

As the equivalent admittance of the AC grid is reduced from 10pu to 0.5pu, the trajectories of the oscillation modes change as shown in Figure 11.

It can be seen that as the equivalent admittance of the AC grid decreases, oscillation modes 1 and 2 are significantly affected, oscillation modes 3 and 4 are slightly affected and oscillation mode 5 is unaffected; oscillation mode 1 gradually shifts to the right, damping and stability decrease, which are consistent with the results of the sensitivity analysis. When the equivalent conductance of the AC grid is reduced to 1.1pu, oscillation mode 1 enters the right half-plane and the system becomes unstable.

As the length of the 500kV transmission line increases from 0.1pu to 4pu, the trajectories of the oscillation modes change as shown in Figure 12.

It can be seen that as the length of the 500kV transmission line increases, oscillation modes 1 and 2 are significantly affected, oscillation modes 3 and 4 are slightly affected and oscillation mode 5 is unaffected; oscillation mode 1 gradually shifts to the left, the damping and stability increase, which are consistent with the results of the sensitivity analysis. When the length of the 500kV transmission line increases to 3.2pu, oscillation mode 1 enters the left half-plane and the system regains stability.

The above device-level analysis shows that oscillation modes 1, 3, and 4 are affected by all equipment in the system; oscillation mode 2 is almost unaffected by the wind farm and the 220kV transmission line; and oscillation mode 5 is almost unaffected by the AC grid, the LCC-HVDC, and the 500KV transmission line. For the dominant oscillation

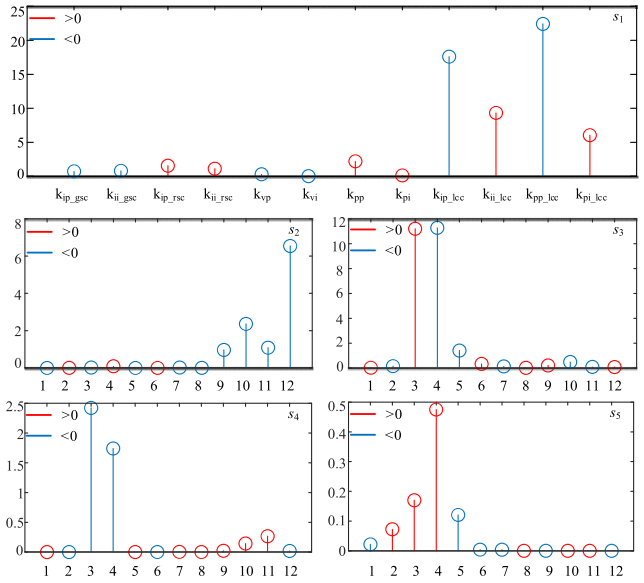

FIGURE 13. Parameter sensitivity (Y-units: -1/s).

mode 1, when the number of wind turbines increases or the equivalent admittance of the AC grid decreases or the length of the transmission line decreases, the damping decreases, and the system stability decreases.

3) PARAMETER-LEVEL OSCILLATION MODE SENSITIVITY

From Figures 2 and 3, it can be seen that there are six PI control loops in the system, with a total of 12 control parameters, the specific symbols are defined in Table 7 and Table 8. The oscillation mode sensitivity of each control parameter is calculated according to (21) and the standardized results are shown in Figure 13. It can be seen that the control parameters of the LCC-HVDC have significant effects on oscillation modes 1 and 2, slight effects on oscillation modes 3 and 4, and no effects on oscillation mode 5; the control parameters of the wind farm have significant effects on oscillation modes 3 to 5, slight effects on oscillation mode 1, and almost no effects on oscillation mode 2.

For the dominant oscillation mode 1, the sensitive control parameters mainly include k_{ip_lcc}, k_{ii_lcc}, k_{pp_lcc}, and k_{pi_lcc}, all of which are control parameters of the LCC-HVDC, while the oscillation mode sensitivity of control parameters of the wind farm is relatively small. The sensitivity of k_{pp_lcc} is the largest, indicating that the change of this parameter has the greatest degree of influence on oscillation mode 1; the sensitivity of k_{ip_lcc} and k_{pp_lcc} is less than 0, indicating that an increase of this parameter will make the real part of oscillation mode 1 decreases, damping and the stability margin of oscillation mode 1 increase; the sensitivity of k_{ii_lcc} and k_{pi_lcc} is greater than 0, indicating that a decrease of the parameter will make the real part of oscillation mode 1 decrease, the damping and the stability margin of oscillation mode 1 increase.

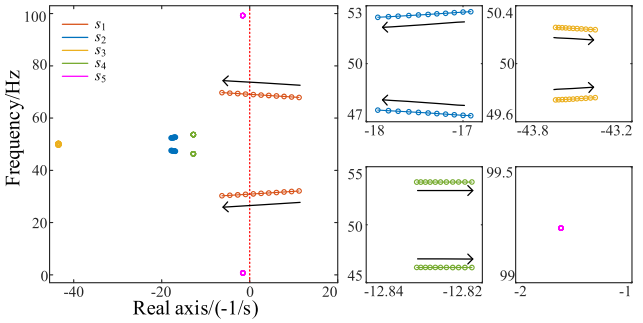

FIGURE 14. System oscillation mode trajectories diagram (k_{ip_lcc}).

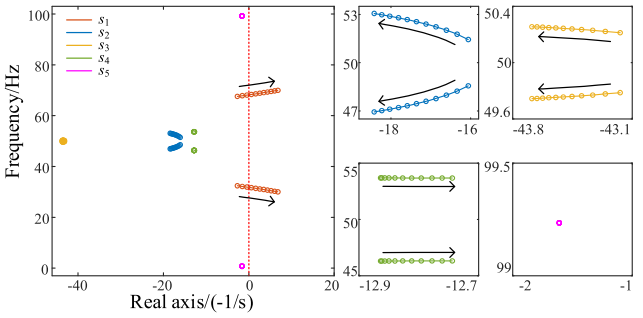

FIGURE 15. System oscillation mode trajectories diagram (k_{ii_lcc}).

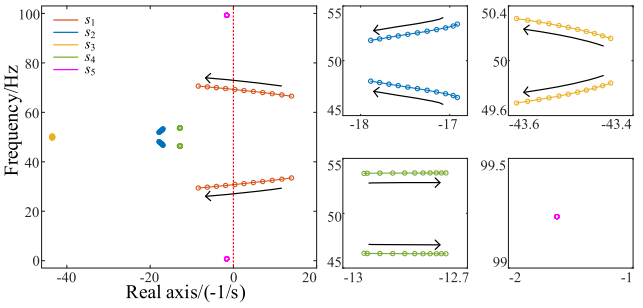

FIGURE 16. System oscillation mode trajectories diagram (k_{pp_lcc}).

Four control parameters of the LCC-HVDC are selected to verify the results of the above analysis. As each control parameter is increased from 0.5pu to 1.5pu, the trajectories of oscillation mode change are shown in Figures 14 to 17.

As can be seen from Figure 14, as k_{ip_lcc} increases, oscillation modes 1 and 2 are significantly affected, oscillation modes 3 and 4 are slightly affected, and oscillation mode 5 is almost unaffected; oscillation mode 1 gradually shifts to the left, damping and stability increase, which are consistent with the results of the sensitivity analysis. When k_{ip_lcc} increases to 1.2pu, oscillation mode 1 enters the left half-plane and the system returns to be stable.

Similarly, the results in Figures 15 to 17 are consistent with the results of the sensitivity analysis. When k_{ii_lcc} is reduced to 0.7pu or k_{pp_lcc} is increased to 1.2pu or k_{pi_lcc} is reduced to 0.5pu, oscillation mode 1 enters the left half-plane and the system returns to be stable.

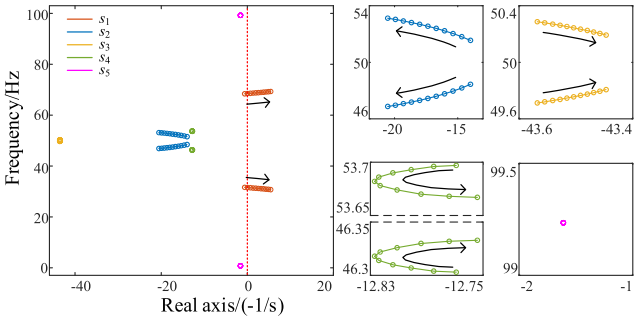

FIGURE 17. System oscillation mode trajectories diagram (k_{pi_lcc}).

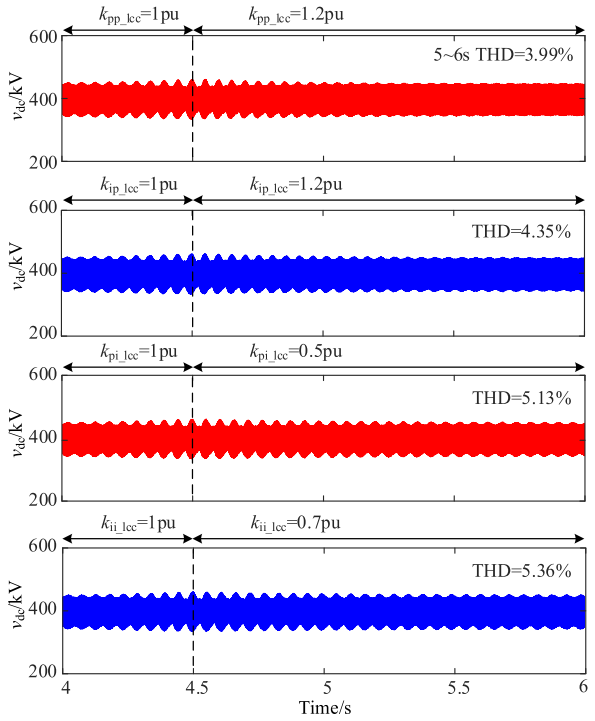

FIGURE 18. Time domain simulation waveform of system.

TABLE 5. Dominant oscillation mode of the system.

Parameter change	Sub-band	Super-band
k_{pp_lcc}=1.2pu	-1.87+j30.41×2π	-1.87+j69.59×2π
k_{ip_lcc}=1.2pu	-0.97+j30.81×2π	-0.97+j69.19×2π
k_{pi_lcc}=0.5pu	-0.63+j31.61×2π	-0.63+j68.39×2π
k_{ii_lcc}=0.7pu	-0.45+j31.91×2π	-0.45+j68.09×2π

The above conclusions are verified by time domain simulations. The dominant oscillation modes for the four cases are listed in Table 5. Figure 18 gives the waveforms of the LCC DC voltage. The operating states from 4s to 4.5s in Figure 18 are the same as those from 4s to 4.5s in Figure 4. By changing the corresponding parameters at 4.5s, the system starts to recover stability in all four cases, where the oscillations disappear at different rates due to the different corresponding damping.

The above analysis at the control parameter level shows that oscillation modes 1, 3, and 4 are influenced by all control parameters, with oscillation mode 1 being mainly influenced by the LCC-HVDC control parameters, oscillation modes 3 and 4 being mainly influenced by the wind farm control parameters; oscillation mode 2 is hardly influenced by the wind farm control parameters; oscillation mode 5 is hardly influenced by the LCC-HVDC control parameters. For the dominant oscillation mode 1, when k_{ip_lcc} increases or k_{ii_lcc} decreases or k_{pp_lcc} increases or k_{pi_lcc} decreases, the damping of oscillation mode 1 and the system stability increases.

V. CONCLUSION

This paper proposes an improved quantitative analysis method of oscillation mode for the multi-node system based on the admittance network model, considering the FCC, and investigates the oscillation characteristics and laws of the DFIG-based wind power base with LCC-HVDC transmission. Conclusions can be reached as:

1) The SNAM considering the FCC can obtain the accurate oscillation modes to determine the stability of the multi-node system. Due to the consideration of FCC, the oscillation modes will appear in pairs, with the oscillation frequencies of each pair being symmetrical about the fundamental frequency.

2) The node oscillation participation factor can quantify the participation information of each node accurately. And the multi-level oscillation mode sensitivity can portray the quantitative relationships between the multi-level factors and the oscillation mode to reveal the system oscillation laws.

3) The dominant oscillation mode 1 is the result of the combined effects of the LCC-HVDC, the AC grid, and the DFIG-based wind farms. Node 6, to which the LCC-HVDC is connected, has the highest involvement in oscillation mode 1. And the control parameters of the LCC-HVDC have the greatest influence on oscillation mode 1.

Based on the proposed improved method, it can accurately and effectively analyze the system oscillation characteristics and laws, and provide a reference for improving the stability of the system, which has high engineering application value.

APPENDIX

A. INFLUENCE OF THE INITIAL VOLTAGE PHASE

Using the system in section IV to analyze the effect of the initial voltage phase on the stability analysis, Table 6 gives the calculation results of the dominant oscillation mode 1 when k_{ip_lcc} increases to 1.2pu, it can be seen that when the initial phase is ignored, the system is judged to be unstable operation; when the initial phase is considered, the system is judged to be stable operation. Figure 19 gives the time domain simulation waveform. The system runs in the operation state corresponding to Table 1 from 4s to 4.5s, at this stage the system is unstable. When changing k_{ip_lcc} from 1pu to 1.2pu

TABLE 6. Dominant oscillation mode of the system.

Initial phase	Sub-band	Super-band	Stability
Without	1.13+j31.03×2π	1.13+j68.97×2π	Unstable
With	-0.97+j30.81×2π	-0.97+j69.19×2π	Stable

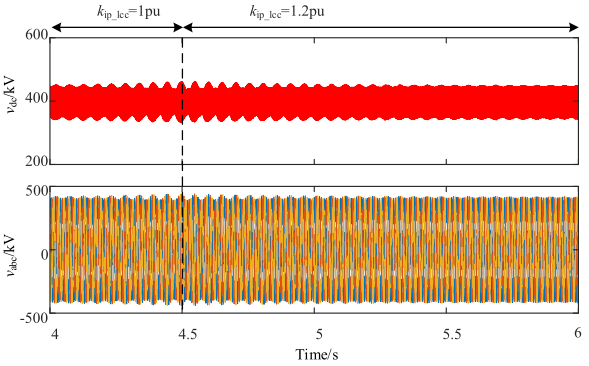

FIGURE 19. Time domain simulation waveform of system.

at 4.5s, it can be seen that the system oscillation starts to weaken, indicating that the system damping is positive in the current operation state, proving that the initial voltage phase cannot be neglected.

B. PARAMETERS OF THE SYSTEM

TABLE 7. Parameter of DFIG-based wind turbine.

Symbol	Parameter	Value
U_s	Rated AC voltage	690 V
P_{DFIG}	Rated Power	1.5 MW
K_e	Turn Ratio	0.37
V_{dc}	Rated DC voltage	1050 V
R_s	Stator resistance	0.0033 Ω
L_{ls}	Stator leakage inductance	0.068 mH
R_r	Rotor resistance	0.0024 Ω
L_{lr}	Rotor leakage inductance	0.105 mH
L_{ms}	Mutual inductance	2.87 mH
C_{dc}	DC capacitor	21.2 mF
C_f	Filter capacitor	0.54 mF
R_f	Filter resistance	0.2 Ω
L_f	Filter inductance	0.5 mH
k_{pp}	PLL proportional gain	282
k_{pi}	PLL integral gain	1100
k_{vp}	Voltage control proportional gain	0.63
k_{vi}	Voltage control integral gain	63.4
k_{ip_rsc}	RSC current control proportional gain	6.12
k_{ii_rsc}	RSC current control integral gain	268
k_{ip_gcc}	GSC current control proportional gain	1.35
k_{ii_gcc}	RSC current control integral gain	394

TABLE 8. Parameter of LCC rectifier station system.

Symbol	Parameter	Value
V_1	Rated AC voltage	500 kV
k_T	Turns ratio	0.34
V_{dc0}	Rated DC voltage	400 kV
P_{nom}	Rated Power	500 MW
R_d	DC link resistance	2.5 Ω
L_d	DC link inductance	0.12 H
C_d	DC link capacitor	26 μF
R_{11}	Filter resistance	3.0557 Ω
L_{11}	Filter inductance	0.0884 H
C_{11}	Filter capacitor	0.947 μF
R_{13}	Filter resistance	2.58 Ω
L_{13}	Filter inductance	0.0632 H
C_{13}	Filter capacitor	0.949 μF
R_{24}	Filter resistance	417.555 Ω
L_{24}	Filter inductance	0.01846 H
C_{24}	Filter capacitor	0.953 μF
G_m	Constant gain	0.0008
T_L	The filter time constant	0.007
k_{pp_lcc}	PLL proportional gain	48
k_{pi_lcc}	PLL integral gain	1400
k_{ip_lcc}	Current control proportional gain	0.53
k_{ii_lcc}	Current control integral gain	52.9

TABLE 9. Parameter of transmission line.

Voltage rate/kV	Resistance/(Ω/km)	Inductance/(mH/km)
220	0.0529	0.977
500	0.0187	0.875

C. WIND FARMS WITH DIFFERENT PARAMETERS

The parameters are consistent with Section IV-A, except for the phase-locked loop proportional gain k_{pp} in four wind farms: wind farm1 (WF1) is 1pu, wind farm2 (WF2) is 1.1pu, wind farm3 (WF3) is 1.2pu and wind farm4 (WF4) is 1.3pu. The analysis results of Case I are shown below, including the oscillation modes of system listed in Table 10, the node oscillation participation factors listed in Table 11, and the

TABLE 10. Oscillation mode of the system.

Oscillation mode	Sub-synchronous band	Super-synchronous band
1	3.25+j30.96×2π	3.25+j69.04×2π
2	-17.37+j47.46×2π	-17.37+j52.54×2π
3	-43.56+j49.76×2π	-43.56+j50.24×2π
4	-12.83+j46.32×2π	-12.83+j53.68×2π
5	-1.61+j0.76×2π	-1.61+j99.24×2π

TABLE 11. Node oscillation participation factors.

Node\s_k	s_1	s_2	s_3	s_4	s_5
1	0.1650	0.15943	0.1813	0.1716	0.1647
2	0.1647	0.15941	0.1827	0.1713	0.1826
3	0.1645	0.15939	0.1837	0.1711	0.1994
4	0.1643	0.15938	0.1846	0.1709	0.2141
5	0.1583	0.15996	0.1491	0.1535	0.1448
6	0.1833	0.20244	0.1186	0.1616	0.09437

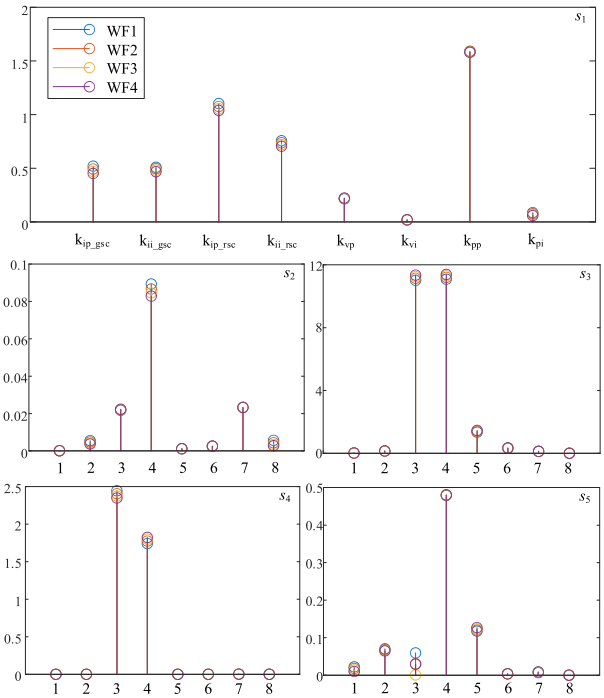

FIGURE 20. Parameter sensitivity of different wind farms (Y-units: -1/s).

parameter-level oscillation mode sensitivities depicted in Figure 20.

REFERENCES

[1] *Renewables 2022*, International Energy Agency IEA, Paris, France, 2022, [Online]. Available: https://www.iea.org/reports/renewables-2022,

[2] H. Li, D. Liu, and D. Yao, "Analysis and reflection on the development of power system towards the goal of carbon emission peak and carbon neutrality," *Proc. CSEE*, vol. 41, no. 18, pp. 6245–6259, Sep. 2021.

[3] X. Yang, Y. Song, G. Wang, and W. Wang, "A comprehensive review on the development of sustainable energy strategy and implementation in China," *IEEE Trans. Sustain. Energy*, vol. 1, no. 2, pp. 57–65, Jul. 2010.

[4] R. Gou, "Research on 1100-kV/5500-A ultra-high voltage thyristor valve key technology and its application," *IEEE Trans. Power Electron.*, vol. 34, no. 11, pp. 10524–10533, Nov. 2019, doi: 10.1109/TPEL.2019.2897745.

[5] R. L. Sellick and M. Åkerberg, "Comparison of HVDC light (VSC) and HVDC classic (LCC) site aspects, for a 500MW 400kV HVDC transmission scheme," in *Proc. 10th IET Int. Conf. AC DC Power Transmiss. (ACDC)*, 2012, pp. 1–6.

[6] X. Jin and H. Nian, "Overvoltage suppression strategy for sending AC grid with high penetration of wind power in the LCC-HVdc system under commutation failure," *IEEE Trans. Power Electron.*, vol. 36, no. 9, pp. 10265–10277, Sep. 2021, doi: 10.1109/TPEL.2021.3066641.

[7] G. Li, Y. Chen, A. Luo, and X. Liu, "Wideband harmonic voltage feedforward control strategy of STATCOM for mitigating subsynchronous resonance in wind farm connected to weak grid and LCC HVDC," *IEEE J. Emerg. Sel. Topics Power Electron.*, vol. 9, no. 4, pp. 4546–4557, Aug. 2021, doi: 10.1109/JESTPE.2020.3027861.

[8] Y. Xu, H. Nian, T. Wang, L. Chen, and T. Zheng, "Frequency coupling characteristic modeling and stability analysis of doubly fed induction generator," *IEEE Trans. Energy Convers.*, vol. 33, no. 3, pp. 1475–1486, Sep. 2018, doi: 10.1109/TEC.2018.2800043.

[9] X. Wang, P. Shi, Y. Liu, H. Nian, Z. Chen, and G. Chen, "Impedance-based stability analysis of LCC-HVDC connected to weak grid considering frequency coupling characteristic," in *Proc. IEEE 5th Int. Electr. Energy Conf. (CIEEC)*, May 2022, pp. 153–157, doi: 10.1109/CIEEC54735.2022.9846154.

[10] M. Á. Cardiel-Álvarez, J. L. Rodriguez-Amenedo, S. Arnaltes, and M. E. Montilla-DJesus, "Modeling and control of LCC rectifiers for offshore wind farms connected by HVDC links," *IEEE Trans. Energy Convers.*, vol. 32, no. 4, pp. 1284–1296, Dec. 2017, doi: 10.1109/TEC.2017.2696261.

[11] A. Yogarathinam, J. Kaur, and N. R. Chaudhuri, "Impact of inertia and effective short circuit ratio on control of frequency in weak grids interfacing LCC-HVDC and DFIG-based wind farms," *IEEE Trans. Power Del.*, vol. 32, no. 4, pp. 2040–2051, Aug. 2017, doi: 10.1109/TPWRD.2016.2607205.

[12] H. Nian, Y. Liu, H. Li, B. Hu, Y. Liao, and J. Yang, "Commutation overlap characteristic modeling and stability analysis of LCC-HVDC in sending AC grid," *IEEE Trans. Sustain. Energy*, vol. 13, no. 3, pp. 1594–1606, Jul. 2022, doi: 10.1109/TSTE.2022.3167106.

[13] M. Wang, Y. Chen, X. Dong, S. Hu, B. Liu, S. S. Yu, H. Ma, X. Zhang, and X. Liu, "Impedance modeling and stability analysis of DFIG wind farm with LCC-HVDC transmission," *IEEE J. Emerg. Sel. Topics Circuits Syst.*, vol. 12, no. 1, pp. 7–19, Mar. 2022, doi: 10.1109/JETCAS.2022.3144999.

[14] A. I. Semlyen, "S-domain methodology for assessing the small signal stability of complex systems in nonsinusoidal steady state," *IEEE Trans. Power Syst.*, vol. 14, no. 1, pp. 132–137, Feb. 1999, doi: 10.1109/59.744501.

[15] S. Gomes, N. Martins, and C. Portela, "Modal analysis applied to S-domain models of AC networks," in *Proc. IEEE Power Eng. Soc. Winter Meeting. Conf.*, 2001, pp. 1305–1310, doi: 10.1109/PESW.2001.917269.

[16] E. Ebrahimzadeh, F. Blaabjerg, X. Wang, and C. L. Bak, "Bus participation factor analysis for harmonic instability in power electronics based power systems," *IEEE Trans. Power Electron.*, vol. 33, no. 12, pp. 10341–10351, Dec. 2018, doi: 10.1109/TPEL.2018.2803846.

[17] Z. Xu, S. Wang, F. Xing, and H. Xiao, "Study on the method for analyzing electric network resonance stability," *Energies*, vol. 11, no. 3, p. 646, Mar. 2018.

[18] H. Nian, Y. Xu, L. Chen, and M. Zhu, "Modeling and analysis of DC-link dynamics in DFIG system with an indicator function," *IEEE Access*, vol. 7, pp. 125401–125412, 2019, doi: 10.1109/ACCESS.2019.2938796.

[19] H. Liu, "HVDC converters impedance modeling and system stability analysis," Ph.D. dissertation, Dept. Elect., Comput. Syst. Eng., Rensselaer Polytech. Inst., Troy, NY, USA, 2017.

[20] J. J. Grainger and W. D. Stevenson, *Power System Analysis*. New York, NY, USA: McGraw-Hill, 1994.

[21] H. Liu, X. Xie, X. Gao, H. Liu, and Y. Li, "Stability analysis of SSR in multiple wind farms connected to series-compensated systems using impedance network model," *IEEE Trans. Power Syst.*, vol. 33, no. 3, pp. 3118–3128, May 2018.

[22] R. L. Boylestad, *Introductory Circuit Analysis*. 13th ed. New York, NY, USA: Pearson, 2015.

[23] G. Strang, *Introduction to Linear Algebra*. 5th ed. London, U.K.: Wellesley-Cambridge Press, 2016.

[24] A. Banner, *The Calculus Lifesaver: All the Tools You Need to Excel at Calculus*. Princeton, NJ, USA: Princeton Univ. Press, 2007.

HAIPAN LI was born in Shanxi, China. He received the B.Eng. degree from Zhejiang University, Hangzhou, China, in 2020, where he is currently pursuing the Ph.D. degree in electrical engineering.

His research interests include the small-signal modeling of renewable generators, their integration to the electric grids and system stability analysis.

HENG NIAN (Senior Member, IEEE) received the B.Eng. and M.Eng. degrees in electrical engineering from the Hefei University of Technology, China, in 1999 and 2002, respectively, and the Ph.D. degree in electrical engineering from Zhejiang University, China, in 2005.

From 2005 to 2007, he was as a Postdoctoral Researcher with the College of Electrical Engineering, Zhejiang University, where he became an Associate Professor, in 2007, and has been a Full Professor, since 2016. From 2013 to 2014, he was a Visiting Scholar with the Department of Electrical, Computer, and System Engineering, Rensselaer Polytechnic Institute, Troy, NY, USA. He has published more than 40 IEEE/IET TRANSACTION articles and holds more than 20 issued/pending patents. His current research interests include optimal design and operation control for wind power generation systems.

YIMING LIU was born in Jining, China. He received the B.Eng. degree in electrical engineering from the Hefei University of Technology, Hefei, China, in 2020. He is currently pursuing the M.Eng. degree in electrical engineering with Zhejiang University.

His research interests include small-signal modeling of LCC-HVDC, its impedance characteristic analysis and system stability analysis.

BIN HU was born in Wenzhou, China. He received the B.Eng. degree in electrical engineering from the Shenyang University of Technology, Shenyang, China, in 2018. He is currently pursuing the Ph.D. degree in electrical engineering with Zhejiang University.

His research interests include phase-locked synchronization methods for wind power generation systems under weak grids, their impedance characteristic analysis and reshaping control strategy.

YUMING LIAO was born in Ganzhou, Jiangxi, China. He received the M.Eng. degree in electronics and power transmission from the Department of Electrical Engineering, Hefei University of Technology, Hefei, China, in 2018. He is currently pursuing the Ph.D. degree in electrical engineering with Zhejiang University, Hangzhou, China.

His research interests include the stability analysis of grid-connected operation and wind power generation systems.

MENG LI (Graduate Student Member, IEEE) was born in Chifeng, China. He received the B.Eng. degree in electrical engineering from Zhejiang University, Hangzhou, China, in 2019, where he is currently pursuing the Ph.D. degree in electrical engineering.

His research interests include the small-signal stability analysis of grid-connected operation and the technology for impedance measurement of renewable generators.